



Scholars Research Library

Der Pharmacia Lettre, 2015, 7 (11):217-227  
(<http://scholarsresearchlibrary.com/archive.html>)



## Theoretical study of molecular properties depending on the photovoltaic parameters of pyridazine derivatives

A. El Assyry<sup>1\*</sup>, A. Hallaoui<sup>2</sup>, F. Rhayt<sup>3</sup>, A. Zarrouk<sup>4</sup>, N. Benchat<sup>4</sup>, H. Oudda<sup>5</sup> and B. Hammouti<sup>4</sup>

<sup>1</sup>Laboratoire d'Optoélectronique et de Physico-chimie des Matériaux, (Unité associée au CNRST), Université Ibn Tofail, Faculté des Sciences, Kénitra, Morocco

<sup>2</sup>Poly-disciplinary Faculty of Taza, Taza Gare, Morocco

<sup>3</sup>Laboratory of Condensed Matter, Faculty of Sciences Ben M'sick (URAC.10), University Hassan II-Mohammedia, Casablanca, Morocco

<sup>4</sup>LCAE-URAC 18, Faculty of Science, First Mohammed University, Oujda, Morocco

<sup>5</sup>Laboratoire des procédés de séparation, Faculté des Sciences, Université Ibn Tofail, Kenitra, Kenitra, Morocco

### ABSTRACT

B3LYP/6-311G(d,p) quantum calculations are performed to optimize geometries and obtain properties depending on the electronic, optical and photovoltaic parameters for some pyridazine derivatives. These novels four organic donor- $\pi$ -acceptor dyes (D- $\pi$ -A) used for dye-sensitized solar cells (DSSC). The results have shown that the polarizable continuum model (PCM) were reasonably capable of predicting the excitation energies, the absorption and the emission spectra of the molecules. The HOMO and LUMO energy levels of these dyes can ensure a positive effect on the process of electron injection and dye regeneration. Gaps energy  $\Delta E_g$ , short-circuit current density ( $J_{sc}$ ), light-harvesting efficiency (LHE), injection driving force ( $\Delta G^{inject}$ ), total reorganization energy ( $\lambda_{total}$ ) and open-circuit photovoltage ( $V_{oc}$ ) permit qualitative predictions about the reactivity of these derivatives.

**Keywords:** DFT, Pyridazine, Oscillator strengths, Electronic properties, Organic Photovoltaic

### INTRODUCTION

Organic photovoltaic solar cells are an important potential of development in the search for low-cost modules for the production of domestic electricity. Recent progress achieved using organic mono-crystal; multilayered thin film and interpenetrated network technologies permit one to expect a very fast increase in the conversion yield of organic solar cells. This will possibly make them a competitive alternative to the various forms of silicon cells. Indeed, the past two years have seen a significant jump in the conversion yield of organic photovoltaic (PV) solar cells, passing from a 1% yield achieved 15 years ago [1], to a 5% yield achieved one year ago [2]. This opens the perspective of seeing very soon, on a typical 5 years time-scale, organic PV cell with solar efficiencies in excess of 10%. The long term objective of such very active research is to reduce the cost of PV modules. In this review, we discuss some of the key technical aspects of the problem. There is no short term ambition to replace silicon, or thin film technologies (a-silicon, CIS or photosensitized cells), but to develop a long term technology based on environmentally safe materials with almost unlimited availability. Such an objective becomes feasible now a day, in the same way as we face the development of efficient organic displays in the electronic industry [3]. Those displays were developed after a 10-year laboratory research effort because they offer a low cost 'easy' technology and a technically attractive alternative to liquid crystal displays. We use the organic light emitting diode (OLED) technology [4] to draw the research guidelines in organic PV cells. Progress in organic PV cells requires a clear understanding of the peculiar physics of amorphous organic semiconductors and devices [5]. We start with the basic understandings of organic semiconductors, and their essential properties such as charge transport. We give indications aimed at selecting efficient organic PV materials and we review some classes of materials used in the different layers of a PV cell. We

then go to an electrical description of organic solar cells. A critical analysis of the physical processes leading to the photovoltaic effect in organic materials permits us to size the maximal and minimal yields achievable using different device structures.

The sunlight is a clean, abundant and virtually limitless energy source which can be used to address the growing global energy needs. Recently, polymer photovoltaic cells (PVCs) have received much attention because of their flexibility, facile processibility, low weight and low production cost [6–8]. Since the 1990s, poly-(p-phenylene vinylene)s (PPVs) and the polythiophenes (PTs) were most studied conjugated polymers with high power conversion efficiencies (PCE) [9, 10]. However, their relatively large band gaps limited the short circuit current ( $J_{sc}$ ), reducing the PCE. In order to further improve the efficiency, low band gap conjugated polymers were developed to better match the solar spectrum and thereby produce higher  $J_{sc}$  [11, 12]. Great progress has been made in PVCs based on bulk-heterojunction (BHJ) networks made of low band gap conjugated polymers and fullerene derivatives in the past few years, and efficiency as high as more than 7% has been reported [13]. In general, the power conversion efficiency (PCE) relies on the open-circuit voltage ( $V_{oc}$ ), the short-circuit current density ( $J_{sc}$ ), and the fill factor ( $FF$ ) of the devices. In PVCs,  $J_{sc}$  is controlled by the matchment between the absorption of the conjugated polymers and the solar spectrum [14]. The  $V_{oc}$  is determined by the difference between the energy levels of lowest unoccupied molecular orbital (LUMO) of the fullerene derivatives (as electron acceptor, A) and the highest occupied molecular orbital (HOMO) of conjugated polymers (as electron donor, D) [15]. Therefore, further improvement in the PCE demands the development of novel conjugated polymers with appropriate energy levels and broader absorption with the solar spectrum. On the other hand, the high charge carrier mobility of polymer semiconductors should also be taken into account [16]. Recent researches showed that the pyridazine system is a promising candidate as a core unit for high performance semi-conductors [17, 18].

Theoretical quantum calculations have been effective tools in the field of chemistry because they can be used to rationalize the properties of known chemical compounds and also predict those of unknown ones to guide observed experimental synthesis. In contrast to experimental results for metal-free organic dyes, the theoretical investigations are still limited. Only few research groups have studied the electronic structures and photophysical properties of dye sensitizers [19, 20], and intra molecular electron dynamic process between dyes and  $TiO_2$  nanocrystalline [21–23]. In this context, the theoretical study of novel pyridazine-based dyes was reported in Fig.1. The central pyridazine was paired through conjugation to an (benzene, chlorobenzene and methyl) and the group ( $C=O$ ,  $-NH-NH_2$ ) as donor groups and linked to substituent as acceptor/anchoring group forming D- $\pi$ -A architecture.

In this study, the electronic structure and optical absorption properties were calculated by using DFT, of four dye sensitizers (Fig.1): 5-[hydroxy(phenyl)methyl]-6-methylpyridazin-3(2H)-one (P1), 4-(2-chlorobenzyl)-6-hydrazino-3-methyl-1,6-dihydropyridazine (P2), 5-(2,6-dichlorobenzyl)-6-methylpyridazin-3(2H)-one (P3) and 5-[(2-chlorophenyl)(hydroxy)methyl]-6-methylpyridazin-3(2H)-one (P4). Based upon the calculated results, we analyzed the role of different electron-donor groups in the tuning the geometries, electronic structures and optical properties. Also, we aimed to see the sensitizer donor effects on the open circuit photovoltage ( $V_{oc}$ ) and the short-circuit current density ( $J_{sc}$ ) of the cell through discussing the key factors affecting  $V_{oc}$  and  $J_{sc}$  with the goal of finding potential sensitizers for use in DSSC.

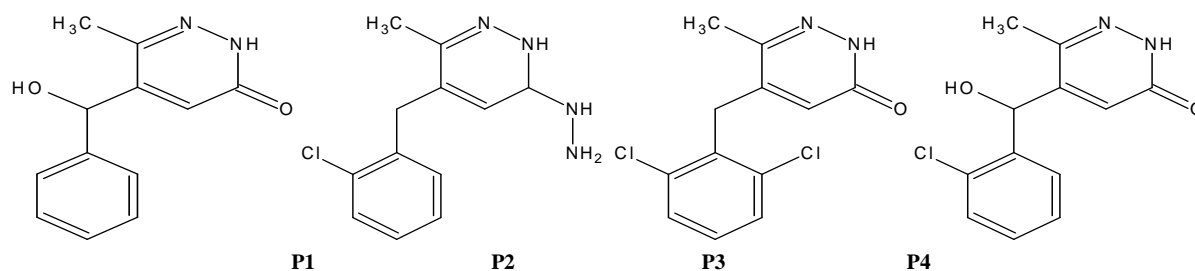


Figure 1: Chemical structure of pyridazine derivatives

## MATERIALS AND METHODS

### Theoretical background

Drawing the current–voltage characteristics of a cell in the dark and under illumination, permits an evaluation of most of its photovoltaic performances as well as its electric behavior [24]. the short circuit current  $I_{sc}$  is the one which crosses the cell at zero applied voltage, it is a function of illumination  $G$ . Charges travel under an internal potential difference typically equal to  $V_{oc}$ ; the open circuit voltage is measured when current in the cell is 0,

corresponding to almost flat valence and conduction bands;  $I_{\max}$  and  $V_{\max}$  values are defined in order to maximize the power  $|I_{\max} \times V_{\max}|$ . This is the maximum power  $P_{\max}$  delivered by the PV cell; fill factor FF is the ratio of the maximum power to the external short and open circuit values:

$$FF = \frac{P_{\max}}{V_{oc} \times I_{sc}} = \frac{V_{\max} \times I_{\max}}{V_{oc} \times I_{sc}}$$

Under monochromatic lightning at a wavelength  $\lambda$ , the yield of electron generated per incident photon; the Internal Photon to Current Efficiency (ICPE) is defined as [25]:

$$IPCE = \frac{J_{sc}}{G \times \lambda} \times \frac{hc}{e}$$

with  $J_{sc}$  the short-circuit current density, or numerically in a very simple manner:  $IPCE = 1.24 J_{sc} / (G \times \lambda)$ . ICPE is the measured parameter in the photovoltaic action spectra.

The external photovoltaic yield  $\eta$  is defined as the ratio of the maximum electric power extracted to the illumination  $G$  times the surface  $S$  of the module:

$$\eta = \frac{P_{\max}}{S \times G}$$

(it is often expressed as a percentage). Conversion yield is the key parameter as concerns cells productivity. It must be evaluated carefully [26], and not be confused with ICPE.

Dark characteristics of the cells are a standard diode one. The sign and value of the applied voltage determines blocking and conducting regimes. The cell conducts when the voltage exceeds a threshold  $V_s$ . An ideal cell can follow the thermionic injection model [27]:

$$I = I_s \left( \exp\left(\frac{eV}{kT} - 1\right) \right)$$

where  $I_s$  is the saturation current under reverse bias.

For the short-circuit current density  $J_{sc}$  in DSSC, it is determined by:

$$J_{sc} = \int_{\lambda} LHE(\lambda) \Phi_{inject} \eta_{collect} d\lambda$$

where  $LHE(\lambda)$  is the light harvesting efficiency,  $\Phi_{inject}$  is the electron injection efficiency, and  $\eta_{collect}$  is the charge collection efficiency. For the same DSSC with only different dyes, it is reasonable to assume that the  $\eta_{collect}$  is a constant. As a result, to shed light onto the relationship between the  $J_{sc}$  and  $\eta$  theoretically, we investigated the  $LHE$ ,  $\Phi_{inject}$  and total reorganization energy ( $\lambda_{total}$ ). To obtain a high  $J_{sc}$ , the efficient sensitizers applied in DSSC should have a large  $LHE$ , which can be expressed as [28]:

$$LHE = 1 - 10^{-f}$$

where  $f$  is the oscillator strength of the dye associate to the wavelength  $\lambda_{\max}$  in the equation. We noticed that the larger oscillating strength obtained, the higher light-harvesting efficiency will have. At the same time, a large  $\Phi_{inject}$  could also guarantee a high  $J_{sc}$ , which is related to the injection driving force  $\Delta G^{inject}$  and evaluated as [28]:

$$\Delta G^{inject} = E^{dye*} + E_{CB}$$

where  $E^{dye*}$  is the oxidation potential energy of the dye in the excited state and  $E_{CB}$  is the reduction potential of the conduction band of  $TiO_2$ , respectively. There, we use in this work  $E_{CB} = -4.0$  eV for  $TiO_2$  [29], which is widely used

in some papers [30-32], and the  $E^{\text{dye}^*}$  can be estimated [31-33]; where  $E^{\text{dye}}$  is the oxidation potential energy of the dye in the ground state, while  $E_{00}$  is an electronic vertical transition energy corresponding to the  $\lambda_{\text{max}}$ . It is generally accepted that there are two schemes to evaluate the  $\Delta G^{\text{inject}}$ , which is relaxed and unrelaxed paths:

$$E^{\text{dye}^*} = E^{\text{dye}} - E_{00}$$

The previous works concluded that the calculation with the unrelax path is reliable [24, 28]. Thus, the electron injection from excited state of dye to the  $\text{TiO}_2$  (CB) is determined by the unrelax path in our investigation. Additionally, the small total reorganization energy ( $\lambda_{\text{total}}$ ) which contains the hole and electron reorganization energy could enhance the  $J_{\text{sc}}$ . Namely, the smaller  $\lambda_{\text{total}}$  value obtained, the faster charge-carrier transport rates will be [25]. So we computed the hole and the electron reorganization energy ( $\lambda_{\text{h}}$  and  $\lambda_{\text{e}}$ ) according to the following formula [34]:

$$\lambda_i = (E_{\text{O}}^{\pm} - E_{\text{I}}^{\pm}) + (E_{\text{I}}^{\text{O}} - E_{\text{O}})$$

where  $E_{\text{O}}^{\pm}$  is the energy of the cation or anion calculated with the optimized structure of the neutral molecule,  $E_{\text{I}}^{\pm}$  is the energy of the cation or anion calculated with the optimized cation or anion structure,  $E_{\text{I}}^{\text{O}}$  is the energy of the neutral molecule calculated at the cationic or anionic state, and the  $E_{\text{O}}$  is the energy of the neutral molecule at ground state.

The equivalent circuit is that of an imperfect current generator, with shunt and series resistances (Fig. 2). Where  $I_{\text{L}}$  is a current source whose intensity depends on  $G$ ,  $R_{\text{s}}$  and  $R_{\text{sh}}$  are the series and shunt resistances,  $R_{\text{L}}$  is the charge resistance of the external circuit [35]. The short circuit current  $I_{\text{sc}}$  is the one which crosses the cell at zero applied voltage; it is a function of illumination  $G$ . Series resistance depends on the material's resistivity, the electrodes resistivity, and the metal-organic interfaces at the electrodes.

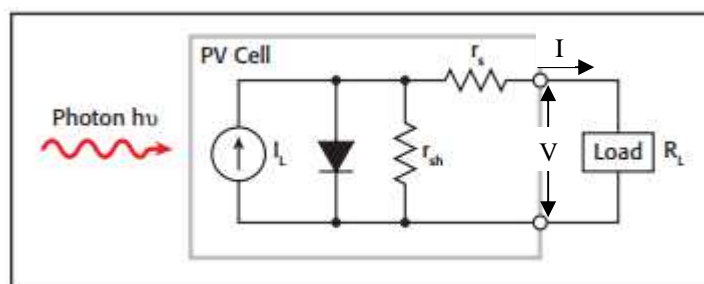


Figure 2: Idealized equivalent circuit of a real photovoltaic cell under light

The shunt resistance (several  $\text{k}\Omega$ ) corresponds to leaks and shorts in the diode. The slope around zero bias is a measure of the shunt resistance [36]. The relation between  $V_{\text{oc}}$  and  $I_{\text{sc}}$  can be determined when it is assumed that:  $R_{\text{s}} = 0$  and  $R_{\text{sh}} = \infty$ , with  $I = 0$  and  $I_{\text{L}} = I_{\text{sc}}$ :

$$V_{\text{oc}} = \frac{nkT}{e} \ln\left(\frac{I_{\text{sc}}}{I_{\text{sc}}} + 1\right)$$

A small shunt resistance  $R_{\text{sh}}$  will reduce  $V_{\text{oc}}$ . Additionally; the cell will not deliver any voltage under low illumination  $G$ .  $I_{\text{sc}}$  is essentially reduced by the series resistance  $R_{\text{s}}$ .

To analyze the relationship between  $V_{\text{oc}}$  (Open-circuit photovoltage) and the  $E_{\text{LUMO}}$  of the dyes based on electron injection from LUMO to the conduction band ( $E_{\text{CB}}$ ) of the semi-conductor  $\text{TiO}_2$ , the  $V_{\text{oc}}$  can be approximately estimated by the analytical relationship [30]:

$$V_{\text{oc}} = E_{\text{LUMO}} - E_{\text{CB}}$$

### Theoretical calculations

All our calculations were performed in the gas phase by using the quantum method DFT (Density Functional Theory) with the hybrid functional of exchange correlation B3LYP [37-40] (Becke three-parameter Lee–Yang–Parr) and the basis set used for all atoms over all calculations is always the basis set of people with dual-polarized (6-31G

(d, p)) [41, 42]. All the optimizations were done without constraint on dihedral angles. The predict energy of excited state and oscillator strengths ( $f$ ) were investigated by using TD-DFT/CAM-B3LYP calculations in chloroform solvent on the fully DFT optimized geometries. We have also examined HOMO, LUMO levels and the energy; the used software of all calculations is Gaussian 09 program [43]. In this paper, the integral equation formalism polarizable continuum model (IEF-PCM) [44-46] was chosen in excitation energy calculations. The cationic and anionic states of dyes were optimized at the B3LYP/6-311G(d,p) level to calculate the total reorganization energies ( $\lambda_{\text{total}}$ ). Polarizable continuum model (PCM) [47, 48] has emerged in the last two decades as the most effective tool to treat bulk solvent effects for both the ground and excited-states.

## RESULTS AND DISCUSSION

### Molecular design and geometry structures

The chemical structures of our compounds (P1, P2, P3 and P4) used in this work are depicted in Fig. 3. All the molecular geometries have been calculated with the B3LYP/6-311G(d,p) level. It was found in other works that the DFT-optimized geometries were in excellent agreement with the data obtained from X-ray analysis [49-51]. The optimized structures for all organic dyes show that they have similar coplanar conformation. We believe that this coplanar molecular-structure should improve the electron transfer from the electron-donor to the electron acceptor through the  $\pi$ -spacer unit for these dyes. The calculated critical bond lengths in all the ground state ( $S_0$ ) and the excited state ( $S_1$ ) permit that these corresponding geometrical parameters in  $S_0$  are very similar with each other. The linkage between the electron-donor and  $\pi$ -conjugated bridge showing especially more C=C character which favors ICT. Indeed, in this D- $\pi$ -A system, the  $\pi$ -conjugated group is employed as the bridge of ICT from the electron-donor to electron-acceptor group. Moreover, upon photoexcitation to the excited state ( $S_1$ ), the bond lengths for these compounds significantly decreased in comparison with those in the ground state ( $S_0$ ). These results indicate that the connection of acceptor group and the  $\pi$ -bridge (pyridazine) is crucial for highly enhanced ICT character, which is important for the absorption spectra red-shift.

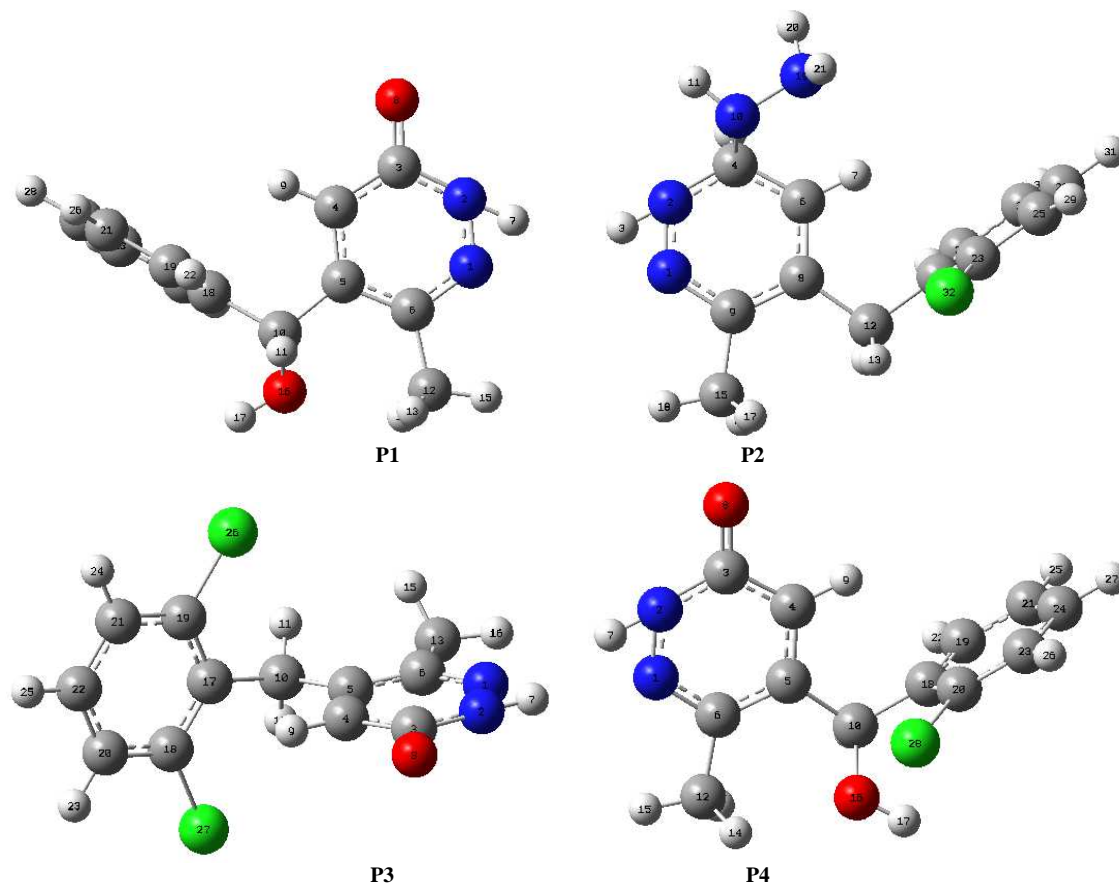


Figure 3: Optimized geometries obtained by B3LYP/6-31G (d,p) of the studied molecules

### Intramolecular charge transfer

In efficient photovoltaic applications, one of the most important features of metal-free organic sensitizers is the intramolecular charge transfer (ICT) from donor to acceptor/anchoring group. The ICT behavior was obtained from the frontier molecular orbital (FMO) contribution [52-55]. Herein, we plotted the electron spatial distribution of

HOMO and LUMO orbitals of all compounds (Fig. 4). In general, the plots of the HOMO and LUMO demonstrated the typical  $\pi$ -type molecular orbital characteristics. Moreover, the HOMO displays an anti-bonding character between two adjacent fragments and bonding character within each unit. The LUMOs exhibit the bonding character between the two adjacent fragments, so the lowest lying singlet states are corresponding to electronic transition of  $\pi$ - $\pi^*$  type [56-59]. As observed in Fig. 4, the pattern of the HOMOs and LUMOs are qualitatively similar with each other, respectively. Moreover, the electron distributions of HOMOs are mainly located in the electron donor to the  $\pi$ -conjugated spacer, while the LUMOs are essentially localized on the conjugation spacer moiety. Therefore, the electronic transitions of all D- $\pi$ -A dyes from HOMO to LUMO could lead to ICT from the donor units to the acceptor/anchoring groups through the conjugated bridge, so that the HOMO-LUMO transition can be classified as a  $\pi$ - $\pi^*$  ICT. Table 1 present the Mulliken Atomic Charge and Natural Charge for all atoms of the compounds studied. The anchoring groups (C=N and C=C) of all compounds has considerable contribution to the LUMOs which could lead to a strong electronic coupling with TiO<sub>2</sub> surface and thus improve the electron injection efficiency, and subsequently enhance the short-circuit current density  $J_{sc}$ .

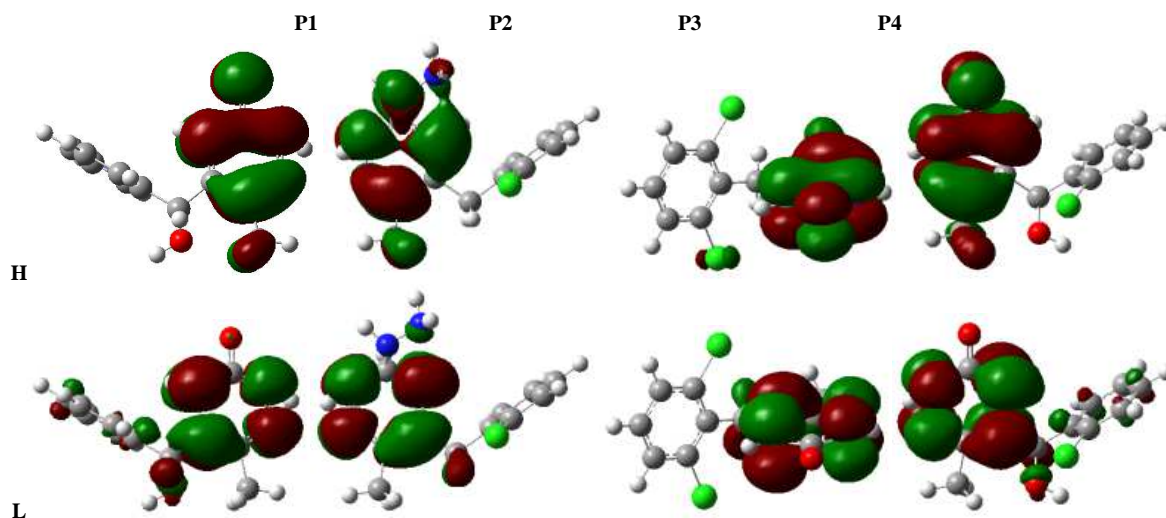


Figure 4: The contour plots of HOMO and LUMO orbital's of the studied compounds

### Molecular orbitals

The analysis of the energy levels of the frontier molecular orbitals (HOMO and LUMO) and the related energy gap ( $\Delta E_g$ ) of our compounds is provided in Table .2, to afford deeper insight about the dependence of the electronic properties on the molecular structure; we note that ( $E_T$ ) present the total energy, ( $\mu$ ) dipole moment, ( $E_{RN}$ ) nuclear repulsion energy and ( $\langle R^{*2} \rangle$ ) Electronic spatial extent. The electron-donating ability of the electron-donor in D- $\pi$ -A dyes has the tendency to influence the electrochemical properties. A D- $\pi$ -A dye with a stronger electron-donating group should give a high HOMO as compared to that with a weaker electron-donor. We have investigated the electron-donor effect on the electronic properties by using different donor groups. According to the analysis of HOMO, the results of these dyes are in order: P2>P3>P1~P4. The P2 and P3 contains the strongest electron-donor group (hydrazino) and (C=O, dichloro) since they have the highest HOMO (-5.430 and -6.565 eV). Dyes P1 and P4 with calculated HOMO energy levels -6.568 eV, have a weak contribution in electron-donor ability due to the fact that they contain a (C=O) group in the electron-donor moiety. The calculated LUMO level for all sensitizers are relatively unaffected by the changes in molecular structure, due to the inclusion of same electron acceptor group (C=N) in these sensitizers, which is less influenced by the change of the donor group. According to the analysis of LUMO, the results of these dyes are in order: P3>P2>P4>P1.

The LUMO energy levels of all dyes are much higher than that of TiO<sub>2</sub> conduction band edge (ca. -4.0 eV) [60]. Moreover, molecules in excited states have a strong ability to inject electrons into TiO<sub>2</sub> electrodes. The HOMO of all dyes is lower than that of  $I/I_3$  (ca. -4.8 eV) [61], therefore, these molecules that lose electrons could be restored by getting electrons from electrolyte. Thus, electron injection of excited molecules and, subsequently, regeneration the oxidized species is energetically permitted. This allows the application of the dyes in dye-sensitized solar cell DSSC.

**Table 1: Mulliken Atomic Charge and Natural Charge for all atoms of the compounds studied**

P1			P2			P3			P4		
Atom	MAC	NC	Atom	MAC	NC	Atom	MAC	NC	Atom	MAC	NC
1 N	-	-	1 N	-	-	1 N	-	-	1 N	-	-
2 N	<b>0.44827</b>	0.28616	2 N	<b>0.44271</b>	0.27927	2 N	<b>0.44665</b>	0.28427	2 N	<b>0.44764</b>	0.28475
3 C	-	-	3 H	-	-	3 C	-	-	3 C	-	-
4 C	<b>0.49778</b>	0.40200	4 C	<b>0.48391</b>	0.45770	4 C	<b>0.49659</b>	0.39957	4 C	<b>0.49731</b>	0.40097
5 C	0.62400	0.50006	5 H	0.42943	0.50992	5 C	0.62541	0.50267	5 C	0.62599	0.50135
6 C	-	-	6 C	0.12286	0.07340	6 C	-	-	6 C	-	-
7 H	0.19600	0.25045	7 H	0.18488	0.19811	7 H	0.18963	0.25618	7 H	0.19275	0.25055
8 O	0.02505	-	8 C	-	-	8 O	0.03089	-	8 O	0.03520	-
9 H	0.27125	0.05928	9 C	0.10348	0.20984	9 H	0.26597	0.03277	9 H	0.27372	0.05724
10 C	0.44647	0.16817	10 N	0.23640	0.27390	10 C	0.44758	0.15672	10 C	0.44706	0.16989
11 H	-	0.51947	11 H	0.02003	-	11 H	-	0.51992	11 H	-	0.51983
12 C	<b>0.52273</b>	-	12 C	0.23798	0.06852	12 H	<b>0.52194</b>	-	12 C	<b>0.52262</b>	-
13 H	0.24685	0.55220	13 H	-	0.10806	13 C	0.23896	0.55142	13 H	0.24208	0.55208
14 H	-	0.27681	14 H	<b>0.43579</b>	-	14 H	-	0.27042	14 H	-	0.27332
15 H	0.05456	0.05920	15 C	0.25238	0.51125	15 H	<b>0.51184</b>	-	15 H	0.07280	0.05528
16 O	0.21495	0.23377	16 H	-	0.33374	16 H	0.24836	0.48408	16 O	0.22206	0.23928
17 H	-	-	17 H	<b>0.50325</b>	-	17 C	0.25774	0.27080	17 H	-	-
18 C	<b>0.58546</b>	0.69704	18 H	0.24320	0.47574	18 C	-	0.27608	18 C	<b>0.58672</b>	0.69739
19 C	0.20091	0.23579	19 N	0.22099	0.26574	19 C	<b>0.60088</b>	-	19 C	0.19885	0.23450
20 C	0.24295	0.26522	20 H	-	0.25525	20 C	0.21502	0.69869	20 C	0.24726	0.26747
21 C	0.20849	0.24401	21 H	<b>0.59825</b>	-	21 C	0.21850	0.24184	21 C	0.20921	0.24452
22 H	-	-	22 C	0.19571	0.69265	22 C	0.22919	0.24259	22 H	-	-
23 C	<b>0.55716</b>	0.68056	23 C	0.20432	0.22818	23 H	0.10728	0.25753	23 C	<b>0.53973</b>	0.67371
24 H	0.36091	0.45124	24 C	0.21399	0.23325	24 H	-	-	24 C	0.36296	0.45131
25 C	-	-	25 C	-	0.24847	25 H 26	0.36030	0.06224	25 H	0.01665	-
26 H	0.04229	0.10041	26 C	<b>0.53082</b>	-	Cl	-	-	26 H	-	0.10825
27 H	-	-	27 H	0.25906	0.70474	27 Cl	0.34768	0.06128	27 H	0.18252	-
28 H	0.19081	0.23320	28 C	0.29363	0.33638	-	-	-	28 Cl	-	0.22419
-	-	-	29 H	0.06086	0.37003	-	0.14013	0.05362	-	0.35843	-
0.18268	0.23323	-	30 H	-	-	-	-	-	-	-	0.06483
0.17832	0.23455	-	31 H 32	0.35137	0.04564	-	0.14082	0.23687	-	0.17894	-
0.18888	0.24487	-	Cl	-	-	-	-	-	-	0.19852	0.23563
-	-	-	-	0.17717	0.05964	-	0.17220	0.23636	-	-	0.25171
0.17869	0.23405	-	-	-	-	-	0.22153	-	-	0.14053	-
0.20319	0.25647	-	-	0.14321	0.22544	-	0.22136	0.23041	-	-	0.23585
-	-	-	-	-	-	-	0.21202	0.26667	-	0.17609	-
0.18159	0.23790	-	-	0.18189	0.24019	-	0.19374	0.26647	-	0.20002	0.23175
0.19376	0.24858	-	-	0.19442	-	-	0.19509	0.26180	-	0.21863	0.25250
0.19475	0.24910	-	-	-	0.23812	-	-	0.02642	-	0.20412	0.26465
0.19390	0.24826	-	-	0.18018	0.25132	-	-	0.02780	-	0.19373	0.25559
-	-	-	-	0.20733	-	-	-	-	-	-	0.03602
-	-	-	-	0.18971	0.24234	-	-	-	-	-	-
-	-	-	-	0.19281	0.25814	-	-	-	-	-	-
-	-	-	-	0.17200	0.24656	-	-	-	-	-	-
-	-	-	-	-	0.24946	-	-	-	-	-	-
-	-	-	-	-	0.01117	-	-	-	-	-	-

The energy gap for these compounds was obtained by the differences of HOMO and LUMO energy levels using B3LYP/6-311G(d,p) and the results are listed in Table. 2. The order of the  $\Delta E_g$  is: P2<P1<P4<P3. With the HOMO–LUMO gap decrease, more photons at the longer-wavelength side would be absorbed to excite the electrons into the unoccupied molecular orbital, which increases the short-circuit current density and further enhances the conversion efficiency of the corresponding solar cell. The ranges of  $\Delta E_g$  are about 2.17–3.36 eV; we may conclude that these dyes have the potential to be employed in the DSSC application.

**Table 2: Optical and electrical parameters for all compounds**

Dye	$E_{\text{HOMO}}$ (eV)	$E_{\text{LUMO}}$ (eV)	$\Delta E_g$ (eV)	$E_T$ (eV)	$\mu$ (Debye)	$E_{\text{RN}}$ (Hartree)	$\langle R^{*2} \rangle$ (au)
P1	-6.568	-3.271	3.297	-19599	5.6846	1052	3781
P2	-5.430	-3.260	2.170	-31000	3.1075	1323	4560
P3	-6.565	-3.202	3.363	-42456	4.8772	1402	4744
P4	-6.568	-3.268	3.300	-32045	6.0986	1313	4229

### Optical properties

The excitation energy and UV-Vis absorption spectra for the singlet–singlet transition of all sensitized dyes were simulated using TDDFT with CAM-B3LYP functional. The computed vertical excited singlet states, transitions energies and oscillator strength of all sensitized dyes in solvent media are tabulated in Table 3. The simulated

absorption spectra data of the studied compounds obtained at the IEF-PCM/TD-CAM-B3LYP/6-311G(d,p) level, the spectra show similar profile for all dyes; they present a main intense band at higher energies from 355 to 378 nm. The most intense contribution to the main band is an excitation from the HOMO to LUMO orbital in solvent as the second singlet excitation.

On the other hand, the position related to the gap between HOMO and LUMO levels, and the width of the first band in the spectrum are the two first parameters that can be related to the dye efficiency, since the absorption shift to lower energies favors the light harvesting process. Herein, the first vertical excitation energies ( $E_{ex}$ ) of the compounds are in decreasing order: P3>P1>P4>P2 showing that there is a bathochromic shift when passing from P3 to P2. The absorption spectra of P4 show slight blue-shift with less decreased oscillator strength, due probably to the electronegativity of the heteroatom in the electron donor groups. The absorption spectra of P2 present the main peak at 377.20 nm. All results of absorption spectra are in good agreement with the energy levels and band gap discussed above.

In order to study the emission photoluminescence properties of the studied compounds, the adiabatic emission spectra were obtained using the optimized geometry of the second excited singlet state at the TDDFT/CAM-B3LYP/6-311G(d,p). The simulated fluorescence wave lengths with the strongest oscillator are presented in Table 3. According to the absorption and emission data, the values of Stokes shift (SS) for all dyes were obtained. The emission spectra arising from  $S_1$  state is assigned to  $\pi^*\rightarrow\pi$  and LUMO $\rightarrow$ HOMO transition character for all molecules. Through analyzing the transition configuration of the fluorescence, we found that the calculated fluorescence is just the reverse process of the lowest lying absorption. Moreover, the observed red shifted emission of the photoluminescence (PL) spectra in order: P3<P1<P4<P2 when passing from P3 to P2 is in reasonable agreement with the obtained results of absorption. Furthermore, the Stokes shift of these dyes is found to be in the range 107.88 and 112.11 nm. The P2 emitted at higher wave-lengths (489.31 nm) with strongest intensity ( $f = 0.0568$ ), and was also characterized by larger Stokes shift (112.11 nm). These encouraging optical properties suggest that P2 with (hydrazino) electron-donor will be the best candidate in the DSSC devices.

**Table 3: Absorption and Emission spectra data for all dyes obtained with PCM-CAM-B3LYP/6-311G(d,p)**

Dye	Absorption				Emission						
	Main composition	$E_{ex}$ (eV)	$\lambda_{max}$ (nm)	$f$	Main composition	$E_{ex}$ (eV)	$\lambda_{max}$ (nm)	$f$	SS (nm)		
P1	H $\rightarrow$ L	0.44	3.457	358.63	0.0408	L $\rightarrow$ H	0.46	2.95	467.52	0.0439	108.89
P2	H $\rightarrow$ L	0.43	3.286	377.20	0.0537	L $\rightarrow$ H	0.45	2.78	489.31	0.0568	112.11
P3	H $\rightarrow$ L	0.46	3.486	355.59	0.0402	L $\rightarrow$ H	0.48	2.98	463.47	0.0433	107.88
P4	H $\rightarrow$ L	0.45	3.445	359.89	0.0396	L $\rightarrow$ H	0.47	2.94	468.84	0.0427	108.95

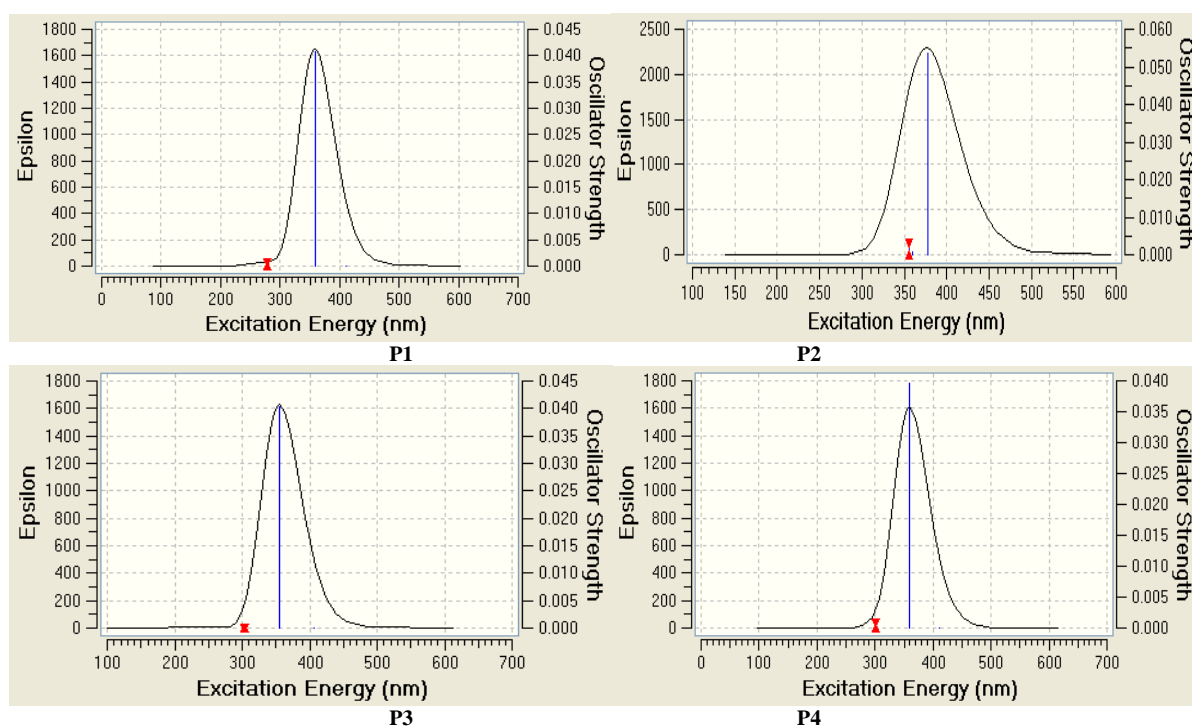


**Figure 5: Simulated absorption spectra of all dyes**

Figure 5 present the simulated absorption spectra of all compounds (oscillator strength and epsilon as a function of wavelength); since the table 4 present the excitation energies and oscillator strengths in deferent exited state.

**Table 4: Excitation energies and oscillator strengths for all compounds**

Excited State	P1			P2			P3			P4		
	E <sub>ex</sub> (eV)	λ (nm)	f	E <sub>ex</sub> (eV)	λ (nm)	f	E <sub>ex</sub> (eV)	λ(nm)	f	E <sub>ex</sub> (eV)	λ(nm)	f
1	3.0207	410.45	0.0000	3.2869	377.20	0.0537	3.0436	407.36	0.0000	3.0159	411.10	0.0000
2	3.4572	358.63	0.0408	3.4443	359.97	0.0007	3.4868	355.59	0.0402	3.4450	359.89	0.0396
3	4.4369	279.44	0.0006	3.4853	355.74	0.0029	4.0731	304.40	0.0001	4.1233	300.69	0.0008

### Photovoltaic properties

The electronic injection free energy  $\Delta G^{\text{inject}}$ , ground  $E^{\text{dye}}$  and excited  $E^{\text{dye}^*}$  state oxidation potentials computed for our compounds are represented in Table 5. Based on Koopman's theorem, ground state oxidation potential energy is related to ionization potential energy.  $E^{\text{dye}}$  can be estimated as negative  $E_{\text{HOMO}}$  [62].  $E^{\text{dye}^*}$  of all dyes is increasing order: P2<P4<P1<P3. It shows that the most convenient oxidizing species is P2 while P3 is the worst. All  $\Delta G^{\text{inject}}$  estimated is in negative value for all sensitizers, thus the electron injection from the dye to TiO<sub>2</sub> is spontaneous. As seen from Table 5 and Fig. 6(b) the calculated ( $-\Delta G^{\text{inject}}$ ) are decreased in the order: P2>P4>P1>P3. It shows that P2 has the largest ( $-\Delta G^{\text{inject}}$ ) value while P3 has the smallest.

Another factor related to efficiency of DSSC is the performance of the dyes responsible of the incident light. Based on the LHE of the dyes, the value has to be as high as possible to maximize the photocurrent response. The LHE values for all dyes are in narrow range 0.087–0.116, but increase slightly with increasing the conjugation length (Fig. 6(a)) in the order: P2>P1>P3>P4. This means that all the sensitizers give similar photocurrent.

**Table 5: Estimated electrochemical parameters for all compounds**

Dye	$E^{\text{dye}}$ (eV)	$E^{\text{dye}^*}$ (eV)	$\Delta G^{\text{inject}}$ (eV)	LHE	$\lambda_{\text{total}}$ (eV)	$V_{\text{oc}}$ (eV)
P1	6.56	3.82	-0.18	0.089	0.47	0.729
P2	5.43	2.75	-1.25	0.116	0.38	0.740
P3	6.56	3.95	-0.05	0.088	0.56	0.798
P4	6.56	3.81	-0.19	0.087	0.44	0.732

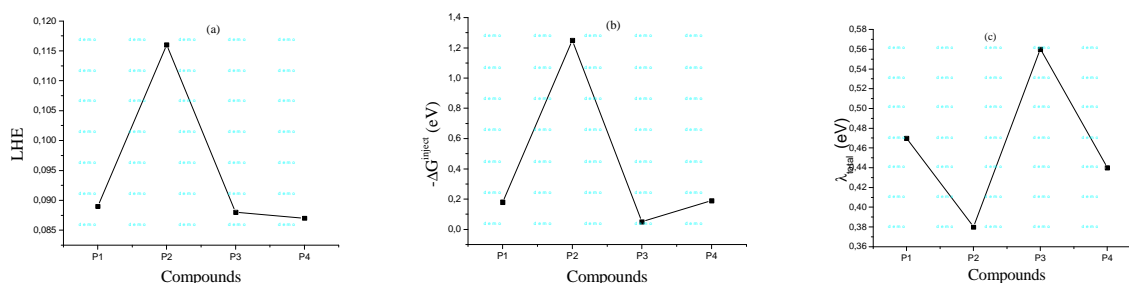


**Figure 6: Critical parameters influenced  $J_{\text{sc}}$  along of investigated sensitizers: (a) the light-harvesting efficiency, (b) the electronic injection free energy and (c) the reorganization energy  $\lambda_{\text{total}}$ .**

As we know, besides the reaction free energy, the reorganization energy  $\lambda_{\text{total}}$  could also affect the kinetics of electron injection. So, the calculated  $\lambda_{\text{total}}$  is also important to analyze the relationship between the electronic structure and the  $J_{\text{sc}}$ . The small  $\lambda_{\text{total}}$  which contains the hole and electron reorganization energy could enhance the  $J_{\text{sc}}$ . As seen from Table 5 and Fig. 6(c) the calculated  $\lambda_{\text{total}}$  of all dyes are increased in the order: P2<P4<P1<P3. It shows that dye P2 possesses the smallest total reorganization energy while dye P3 has the largest. As a result, dye P2 exhibits a favorable  $J_{\text{sc}}$  due to the relative similar LHE, larger  $\Delta G^{\text{inject}}$  and smaller  $\lambda_{\text{total}}$ . At the same time,  $\Delta G^{\text{inject}}$  and  $\lambda_{\text{total}}$  are more important to govern the  $J_{\text{sc}}$  mostly.

As discussed in section, we know that besides the short-circuit current density  $J_{\text{sc}}$  the overall power conversion efficiency  $\eta$  also could be influenced by the open-circuit voltage ( $V_{\text{oc}}$ ). Therefore, between two dyes with similar structures, the electron injection would be more efficient for that dye with the higher excited state related to the semi-conductor conduction band edge (i.e. higher  $V_{\text{oc}}$ ). It was found that  $V_{\text{oc}}$  of all dyes (Table 5) is in the range 0.729–0.798 eV and in decreasing order: P1<P4<P2<P3. It shows that P3 has the largest  $V_{\text{oc}}$  values, while P2, P4 and P1 have the smallest.

As a consequence of the above data, we could draw a conclusion that the large LHE and  $\Delta G^{\text{inject}}$  as well as small  $\lambda_{\text{total}}$  and  $V_{\text{oc}}$  could have a high efficiency. Thus, the performance of DSSC sensitized by dye P2 might be superior to the other dyes, due to its favorable performances of the above factors based on our computed results.

### CONCLUSION

In this study, we used the DFT/B3LYP level to analyze the geometries and electronic properties of new molecules based on pyridazine with several structures. The modification of chemical structures can greatly modulate and improve the electronic and optical properties of pristine studied materials. The optoelectronic properties of these new conjugated materials have been computed using 6-31G (d, p) basis set at B3LYP level. The concluding remarks are: • the appropriate functional to predict the electronics properties is B3LYP; • the appropriate functional to predict the optical properties is CAM-B3LYP; • the absorption properties have been obtained by using TD-DFT method, the obtained absorption maximums are in the range 355 to 377 nm; • the calculated band gap ( $\Delta E_g$ ) of the studied molecules was in the range 2.170 to 3.363 eV; • the calculated values of  $V_{\text{oc}}$  of the studied molecules range from 0.729 to 0.798 eV; • the 4-(2-chlorobenzyl)-6-hydrazino-3-methyl-1,6-dihydropyridazine (P2) dye was found to be the best photo-sensitizer for use in DSSC,

These values are sufficient for an efficient electron injection; all the studied molecules can be used as organic solar cells. Finally, the procedures of theoretical calculations can be employed to predict the optoelectronic properties on the other compounds, and further to design novel materials for organic solar cells.

### REFERENCES

- [1] C.W. Tang, *Appl. Phys. Lett.*, **1986**, 48, 183.
- [2] J.H. Schön, Ch. Kloc, B. Batlogg, *Appl. Phys. Lett.*, **2000**, 77, 2473.
- [3] P. Le Barny, V. Dentan, H. Facoetti, M. Vergnolle, G. Vériot, B. Servet, C. R. Acad., *Sci. Paris Sér. IV*, **2000**, 1, 493.
- [4] J. Kalinowski, Electroluminescence in organics, *J. Phys. D* 32, **1999**, R179.
- [5] J. Simon, J.-J. André, *Molecular Semiconductors: Photoelectrical Properties and Solar Cells*, Springer, **1985**.
- [6] B. C. Thompson and J. M. J. Frechet, *Angew. Chem., Int. Ed.*, **2008**, 47, 58.
- [7] F. C. Krebs, S. A. Gevorgyan and J. Alstrup, *J. Mater. Chem.*, **2009**, 19, 5442.
- [8] F. C. Krebs, J. Fyenbo and M. Jørgensen, *J. Mater. Chem.*, **2010**, 20, 8994.
- [9] C. J. Brabec, S. E. Shaheen, C. Winder, N. S. Sariciftci and P. Denk, *Appl. Phys. Lett.*, **2002**, 80, 1288.
- [10] G. Li, V. Shrotriya, Y. Yao and Y. J. Yang, *Appl. Phys. Lett.*, **2005**, 98, 437041.
- [11] F. Padinger, R. S. Rittberger and N. S. Sariciftci, *Adv. Funct. Mater.*, **2003**, 13, 85.
- [12] W. L. Ma, C. Y. Yang, X. Gong, K. Lee and A. J. Heeger, *Adv. Funct. Mater.*, **2005**, 15, 1617.
- [13] Y. Y. Liang, Z. Xu, J. B. Xia, S. T. Tsai, Y. Wu, G. Li, C. Ray and L. P. Yu, *Adv. Mater.*, **2010**, 22, E135.
- [14] K. L. Mutolo, E. I. Mayo, B. P. Rand, S. R. Forrest and M. E. Thompson, *J. Am. Chem. Soc.*, **2006**, 128, 8108.
- [15] A. Gadisa, M. Svensson, M. R. Andersson and O. Inganäs, *Appl. Phys. Lett.*, **2004**, 84, 1609.
- [16] S. H. Chan, C. P. Chen, T. C. Chao, C. Ting, C. S. Lin and B. T. Ko, *Macromolecules*, **2008**, 41, 5519.
- [17] J.H. He, W. Mao, G.Q. Xu and E.S. Tok, *Nat. Commun.* **2014**, 5, 3721.
- [18] A. El Assyry, A. Hallaoui, R. Saddik, N. Benchat, B. Benali, A. Zarrouk, *Der Pharm. Lett.*, **2015**, 7(9), 295.
- [19] A. El Assyry, A. Hallaoui, F. Abrighach, R. Touzani, A. Zarrouk, A. Lamhamdi, *Der Pharm. Lett.*, **2015**, 7(9), 151.
- [20] S. Abouricha, EM. Rakib, N. Benchat, M. Alaoui, H. Allouchi, B. El Bali, *Synth. Commun.* **2005**, 35, 2213.
- [21] A. El Assyry, R. Jdaa, B. Benali, M. Addou, A. Zarrouk, *J. Mater. Environ. Sci.*, **2015**, 6, 2612.
- [22] Dessì A., Consiglio G.B., Calamante M., Reginato G., Mordini A., Peruzzini M., Taddei M., Sinicropi A., Parisi M. L., Biani F. F., Basosi R., Mori R., Spatola M., Bruzzi M., Zani L., *Eur. J. Org. Chem.* **2013**, 2013, 1916.
- [23] Zhang C.R., Liu Z.J., Chen Y.H., Chen H. S., Wu Y.Z., Yuan L.H., *J. Mol. Struct. (Theochem)*, **2009**, 899, 86.
- [24] L. Sicot, Étude et réalisation de cellules photovoltaïques en polymère, *PhD thesis*, Orsay, **1999**.
- [25] J.-M. Nunzi, *C. R. Physique*, **2002**, 3, 523.
- [26] J. Rostalski, D. Meissner, *Solar Energy Mater. Solar Cells*, **2000**, 61, 87.
- [27] S.M. Sze, *Physics of Semiconductor Devices*, Wiley, **1981**.
- [28] Z.L. Zhang, L.Y. Zou, A.M. Ren, Y.F. Liu, J.K. Feng, C.C. Sun, *Dyes Pigm.* **2013**, 96, 349.
- [29] J.B. Asbury, Y.Q. Wang, E. Hao, H. Ghosh, T. Lian, *Res. Chem. Intermed.* **2001**, 27, 393.
- [30] J. Zhang, H.B. Li, S.L. Sun, Y. Geng, Y. Wu, Z.M. Su, *J. Mater. Chem.* **2012**, 22, 568.
- [31] J. Zhang, Y.H. Kan, H.B. Li, Y. Geng, Y. Wu, Z.M. Su, *Dyes Pigm.* **2012**, 95, 313.
- [32] W.L. Ding, D.M. Wang, Z.Y. Geng, X.L. Zhao, W.B. Xu, *Dyes Pigm.* **2013**, 98, 125.
- [33] W. Sang-aroon, S. Saekow, V. Amornkitbamrung, *J. Photochem. Photobiol. A* **2012**, 236, 35.
- [34] M.P. Balanay, D.H. Kim, *J. Mol. Struct. Thermochem.* **2009**, 910, 20.

- [35] S.M. Sze, *Physics of Semiconductor Devices*, Wiley, **1981**.
- [36] A. Ricaud, *Photopiles solaires*, Presses polytechniques et universitaires romandes, **1997**.
- [37] A.D. Becke, *J. Chem. Phys.*, **1993**, 98, 5648.
- [38] A.D. Becke, *Phys. Rev. A*. **1988**, 38, 3098.
- [39] A. El Assyry, B. Benali, A. Boucetta, B. Lakhriksi, *J. Mater. Environ. Sci.*, **2014**, 5, 1860.
- [40] C. Lee, W. Yang, R.G. Parr, *Reviews B*, **1988**, 37, 785.
- [41] M.S. Gordon, *Chem. Phys. Lett.*, **1980**, 76, 33.
- [42] R.J. Magyar, S. Tretiak, *J. Chem. Theory. Comput.*, **2007**, 3, 976.
- [43] M.J. Frisch, G.W. Trucks, H.B. Schlegel, G.E. Scuseria, M.A. Robb, J.R. Cheeseman et al., Gaussian 09, revision A.02, Gaussian, Inc., Pittsburgh, PA, **2009**.
- [44] J. Tomasi, B. Mennucci, R. Cammi, *Chem. Rev.* **2005**, 105, 2999.
- [45] A. El Assyry, B. Benali, A. Boucetta, D. Mondieig, *Res. Chem. Intermed.* **2014**, 40, 1043.
- [46] M. Cossi, V. Barone, *J. Chem. Phys.* **2001**, 115, 4708.
- [47] D. Ben Hmamou, R. Salghi, A. Zarrouk, H. Zarrak, B. Hammouti, S. S. Al-Deyab, A. El Assyry, N. Benchat, M. Bouachrine, *Int. J. Electrochem. Sci.* **2013**, 8, 11526.
- [48] C. Adamo, V. Barone, *Chem. Phys. Lett.* **2000**, 330, 152.
- [49] D. Mondieig, Ph. Negrier, J. M. Leger, L. Lakhriksi, A. El Assyry, B. Lakhriksi, E. M. Essassi, B. Benali, A. Boucetta, *Russ. J. Phys. Chem. A*. **2015**, 89, 807.
- [50] Ph. Négrier, D. Mondieig, J. M. Léger, B. Benali, Z. Lazar, A. Boucetta, A. ElAssyry, B. Lakhriksi, C. Jermoumi, M. Massoui, *Anal. Sci.* **2006**, 22, 175.
- [51] D. Mondieig, Ph. Négrier, J. M. Léger, B. Benali, Z. Lazar, A. ElAssyry, C. Jarmouni, B. Lakhriksi, M. Massoui, *Anal. Sci.* **2005**, 21, 145.
- [52] B. Benali, A. El Assyry, A. Boucetta, Z. Lazar, B. Lakhriksi, *Res. Chem. Intermed.* **2015**, 41, 821.
- [53] B. Benali, A. El Assyry, Z. Lazar, A. Boucetta, *J. Mater. Environ. Sci.* **2014**, 5, 426.
- [54] A. El assyry, B. Benali, A. Boucetta, Z. Lazar, B. Lakhriksi, M. Massoui and D. Mondieig, *Spectrosc. Lett.* **2009**, 42, 203.
- [55] B. Benali, Z. Lazar, A. Boucetta, A. El Assyry, B. Lakhriksi, M. Massoui, C. Jermoumi, P. Negrier, J. M. Leger, D. Mondieig, *Spectrosc. Lett.* **2008**, 41, 64.
- [56] B. Benali, A. El Assyry, A. Boucetta, Z. Lazar, B. Lakhriksi, M. Massoui, D. Mondieig, *Spectrosc. Lett.* **2007**, 40, 893.
- [57] B. Benali, Z. Lazar, K. Elblidi, B. Lakhriksi, M. Massoui, A. Elassyry and C. Cazeau-Dubroca, *J. Mol. Liq.* **2006**, 128, 42.
- [58] B. Benali, A. Boucetta, Z. Lazar, K. Elblidi, A. El Assyry, C. Cazeau-Dubroca, *J. Mol. Liq.* **2006**, 126, 29.
- [59] A. Elassyry, B. Benali, Z. Lazar, K. Elblidi, B. Lakhriksi, M. Massoui, D. Mondieig, *J. Mol. Liq.* **2006**, 128, 46.
- [60] J.B. Asbury, Y.Q. Wang, E. Hao, H. Ghosh, T. Lian, *Res. Chem. Intermed.* **2001**, 27, 393.
- [61] A. Hagfeldt, M. Grätzel, *Chem. Rev.* **1995**, 95, 49.
- [62] R.G. Pearson, *Inorg. Chem.* **1988**, 27, 734.